Laser Compression and Fragmentation of Metals*

M. A. Meyers[1], H. Jarmakani[1], B. Y. Cao[1], C. T. Wei[1], B. Kad[1],B. A. Remington[2], E. M. Bringa[2], B. Maddox[2],D. Kalantar[2], D. Eder[2], A. Koniges[2]

[1] *U. of California, San Diego, la Jolla, CA, USA*

[2.] *Lawrence Livermore National Laboratory, Livermore, CA, USA*

Abstract: Using the Janus LLNL and Omega facilities, we are using laser energy to generate shock and quasi-isentropic compression of monocrystalline, polycrystalline , and nanocrystalline FCC and BCC metallic specimens(Cu, Ni, V). We have investigated the internal defects generated by experimental and computational (MD) means. By comparing experimentally observed and computationally predicted structures we can obtain new insights into the fundamental deformation mechanisms. We have also investigated the mechanisms of spall initiation, propagation, and fragmentation.

1. INTRODUCTION: LASER COMPRESSION

A number of proposals for dislocation generation in shock compression have been advanced over the years, but none of them have been critically tested. Several models of the physics occurring at the shock front (where the material is rapidly deformed plastically) have emerged over the years: (a)The**Smith interface**, composed of supersonic dislocations originally proposed in 1950 [1] and updated, modified, and quantified by Weertman et al. [2-4]. (b) Conventional **Orowan dislocation multiplication**; Johnson and coworkers [5, 6] have implemented these concepts. (c) **Homogeneous dislocation generation** at or behind the shock front; generation-controlled residual dislocation densities were calculated by Meyers [7, 8]. (d) **Stacking-fault multiplication**; this proposal by Zaretsky [9] attempts to reconcile results of flash X-ray diffraction with stacking-fault generation at the shock front.

In the strain rate range from 10^6 to $10^{10}s^{-1}$, deformation mechanisms are less well understood and conventional deformation mechanisms are not applicable. An additional complexity is introduced by nanostructured metals, in which the mechanisms of plastic deformation are significantly different. Figure 1, based on an Ashby plot, schematically shows a temperature vs. strain rate diagram in which conventional (i.e. known) and extreme (unknown) deformation rate fields are marked. The objective of the research described herein is to employ laser-induced compression identify the deformation mechanisms operating in this unknown regime.

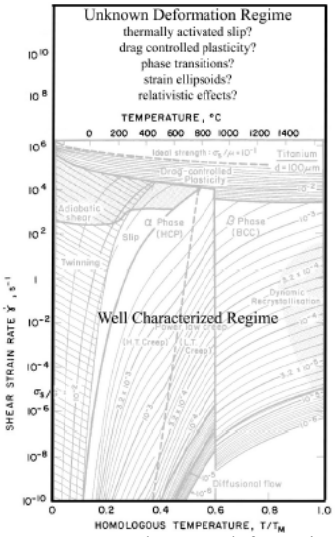

Figure 1: Unknown deformation regimes for laser induced shocked materials.

The regimes obtained by laser shock are indeed extreme and cannot be accessed by other experimental methods. The experimental facilities of Jupiter and Omega enable unique materials experiments. As we embark in the NIF (National Ignition Facility) era, it is imperative to understand the basic physics of plastic deformation of advanced materials in the extreme regimes created under these conditions.

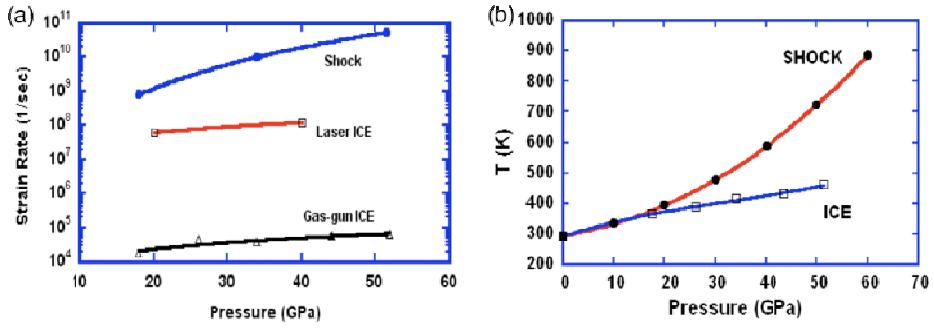

Figure 2: (a) Strain rates in gas gun, laser shock and isentropic compression (b) corresponding residual temperatures as a function of pressure for two cases(from Jarmakani et al.[10]).

The current emphasis on Omega and Jupiter laser experiments is shifting from shock to isentropic compression. There are distinct differences between the two compression

modes, the most important being the strain rates during the loading stage and the maximum temperature.Figure 2(a) [10] shows the strain rates calculated for gas-gun shock and isentropic compression of copper, as well as laser isentropic compression. The strain rates for shock compression are several orders of magnitude higher than for gas-gun isentropic compression. The strain rates in laser isentropic are higher than in gas gun but still significantly lower than in shock. The residual temperatures are also correspondingly different, with shock compression producing temperature rises that lead to melting at pressures much below those for isentropic compression (Fig. 2b).Thus, quasi-isentropic compression is necessary to access the pressure regime of 100 GPa and beyond.

2. SHOCK AND ISENTROPIC COMPRESSION: CHARACTERIZATION

For copper and Cu-Al alloys, it was demonstrated by our group that there are clear differences in the defect structures generated by the two modes of deformation (shock and isentropic). Specifically, the onset of twinning is translated to a higher pressure in isentropic compression. As an illustration, we cite here the predicted transition pressures for copper. The threshold pressure is approximately 15 GPa for shock compression and 30GPa for laser quasi-isentropic-compression[10].

3. SHOCK COMPRESSION: MOLECULAR DYNAMICS MODELING

This section is a summary of the work by Jarmakani et al. [11] and Cao et al.[12]. Molecular Dynamics simulations were carried out using the Large-scale Atomic/Molecular Massively Parallel Simulator (LAMMPS) code [13], a EAM potential developed by Mishin et al. [14,15]. This potential was fitted to give a stacking-fault energy of 125 mJ/m^2 [14] for Ni and 45 mJ/m^2 for Cu [15]. EAM views each atom as embedded in a host lattice consisting of all other atoms. Each atom in the system is viewed as an impurity that is part of a host of all other atoms. The "embedding energy" of the impurity is determined by the electron density of the host before the impurity is added. The energy of an atom or impurity is represented as a function of the electron density at the atom site plus an electro-static interaction due to the host [16]:

$$E_i = F_i(\rho_i(R_i)) + \frac{1}{2}\sum_j \varphi(R_{ij}) \tag{1}$$

whereρ_i is the electron density of the host atom i, φ is the short range electro-static pair potential as a function of the distanceR_{ij} between atoms$i$ and j, and F is the "embedding energy" as a function of the host electron density,ρ_i , induced at site $i$by all other atoms in the system. The total energy is a sum over all individual contributions.

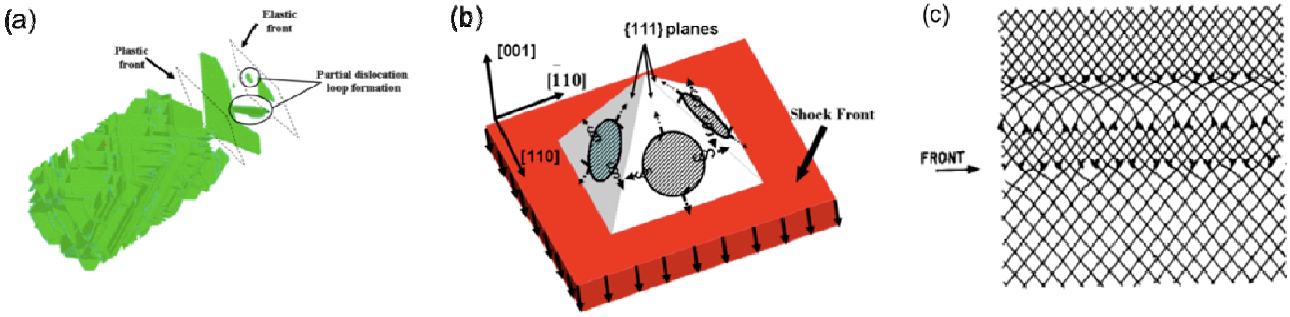

Figure 3: Shock compression of Ni along [001]; U_p=0.786 km/sec (a) Stacking faults, view along longitudinal z direction; (b) schematic representation of partial dislocation loop formation; (c) Dislocation interface as represented by Meyers [7].

For better visualization of defects (dislocations, stacking faults, twins), the "centrosymmetry" parameter is used, to identify defective atoms (dislocation cores and stacking faults). It is of the form [17]:

$$C = \sum_{i=1}^{6} |\vec{r}_i + \vec{r}_{i+6}|^2 \tag{2}$$

wherer_i and r_{i+6} are the vectors from the central atom to the opposite pair of nearest neighbors (6 pairs in fcc system,

i.e. the coordination number). Atoms in perfect fcc lattice positions have a C equal to zero, whereas atoms having

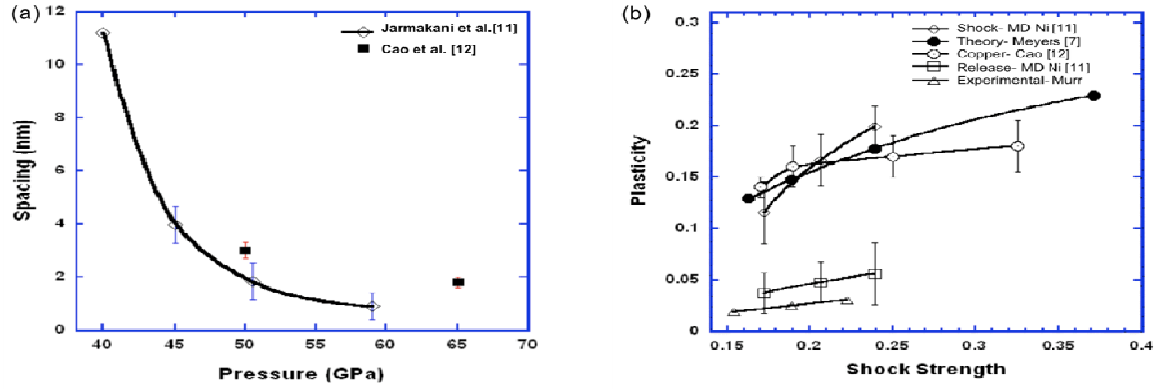

Figure 4: (a) MD computed spacing between stacking faults as a function of pressure for Cu [12] and Ni[11].; (b) Holian-Lomdahl plot with computed (MD) and experimentally observed values [19].

faulty stacking will comprise of a nonzero C value.

The defect spacing as a function of shock pressure was analyzed in order to quantify the induced plasticity, Figure 4 (a). Clearly, the stacking fault spacing decreases as the shock pressure increases. Copper data from Cao et al. [12] and nickel data from Jarmakani et al.[11] are plotted. Holian and Lomdahl [19] introduced two fundamental deformation parameters: shock-induced plasticity and shock strength. Shock-induced plasticity is defined as a_o/l, where $a_o$is the lattice constant, and l is the average lattice spacing between stacking faults. Shock strength is defined as the ratio between particle velocity and speed of sound in the material, U_p/c_o. The shock induced plasticity as a function of shock strength is plotted in Figure 4 (b). MD data on Cu from Cao et al. [12] and on Ni from Jarmakani et al. [11], predictions from the homogeneous nucleation model of Meyers [7], and experimentally measured data from Murr [19] are also shown on the plot. The data shown from Meyers [7] and Murr[20] was extracted from the reported dislocation densities using the equation $L = \sqrt{\rho^{-1}}$, where ρ is the dislocation density and L is the dislocation spacing. Note that the plasticity data from MD results from Cao et al.[12] and Jarmakani et al.[11] are consistent with theoretical calculations by Meyers [7]. The experimentally determined shock plasticity of Ni from Murr [19] is, however, lower than the theoretical and MD results by an order of magnitude. This suggests that relaxation processes are clearly at play in real experiments resulting in lower dislocation densities, as will be shown below. Figure 4 (b) shows the MD plasticity after release whereby an order of magnitude drop is evident, synonymous with the experimental data by Murr [19].

The effect of release in the MD simulations was studied

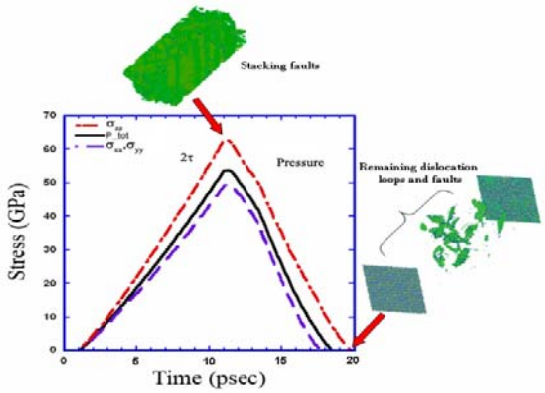

Figure 5:P_{tot}, σ_{xx}, σ_{yy}, σ_{zz} vs. time step, U_p=1.1 km/sec.

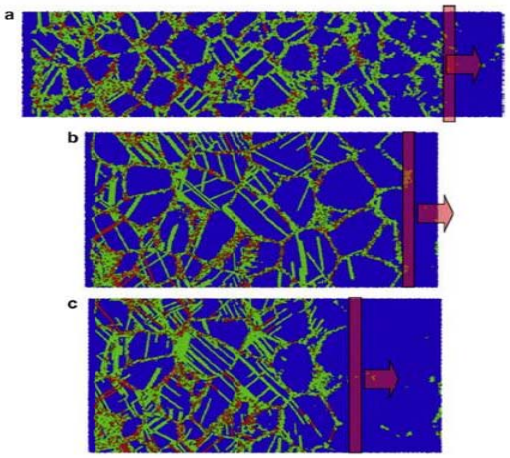

Figure 6: Nanocrystalline Ni (a, b) and Cu (c) shock compressed to particle velocity of U_p=0.67 mm/μsec (a) 5 nm Ni; (b) 10 nm Ni; (c) 10 nm Cu

for comparison with experiments. The total ramp time (loading +unloading) is 20 ps and the pressure was allowed to retract back to zero.The pressure rise due to compression and the accompanying drop due to release are shown in Figure 5 for the case of U_p=1.1 km/sec. Only the defective atoms (light) are shown in the figure.Interestingly, almost all the partial dislocation loops disappear. The spacings between the few remaining stacking faults were measured, and the resulting recovered plasticity was calculated.

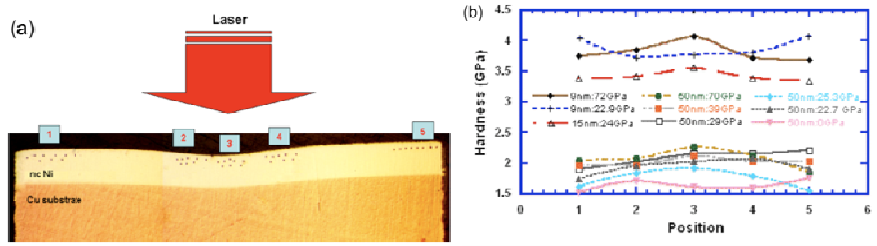

Figure 7: (a) Cross-sectional microhardness measurements from 5 positions beneath crater; (b) Hardness vs. position.

Figure 6 shows three shocked nanocrystalline samples. The color code is as follows: the dark atoms are not displaced and are in their original minimum energy state, the light atoms are displaced by the Burgers vector of a Shockley partial, the red atoms are displaced by a Burgers vector of a perfect dislocation, and the orange atoms are displaced by a Burgers vector larger than that of a perfect dislocation. For the 5 nm grain-sized Ni sample, the total strain contribution due to dislocations is dominated by partials. Partials make up ~ 60 % of the total strain due to dislocations, and perfect dislocations account for ~ 10 %. The contribution due to twinning was 26 %. The total shock strain in the sample was calculated to be ~ 0.13. By subtracting the strain due to dislocations from the total strain, one obtains the strain due to grain-boundary sliding, 0.116; this represents approximately 90 % of the total.

In the case of the 10 nm grain-sized samples, the strain contribution due to partials is 62.6 % for Ni and 56.0 % for Cu. Perfect dislocations account for 17.2 % of the dislocation strain in Ni and 20.6 % in Cu. The twinning contribution is greater in Cu, 19 % as compared to 15.7 % in Ni. This is to be expected since the stacking fault energy of Cu is significantly lower. Grain boundary sliding accounts for approximately 75 % of the total strain in both Ni and Cu, signifying that it becomes more difficult for larger grains to slide past one another under compression. The right hand portion of the simulations do not show the grain boundaries highlighted in light. This is due to the fact that no grain boundary sliding is taking place because the shock front has not yet traveled through that region. The contribution due to partials is comparable in the 5 and 10 nm grain-sized samples, but that from perfect dislocations is greater in the 10 nm samples. Interestingly, the twinning contribution is greater in the 5nm grain-sized sample (5nm Ni: 25.7 %, 10nm Ni: 15.7 %). This result is in agreement with the models proposed by Chen et al. [21] and Zhu et al. [22], where they show that propensity for twinning increases with decreasing grain size. It is also in agreement with mechanisms for deformation of nanocrystalline metals discussed by Meyers et al.[23].

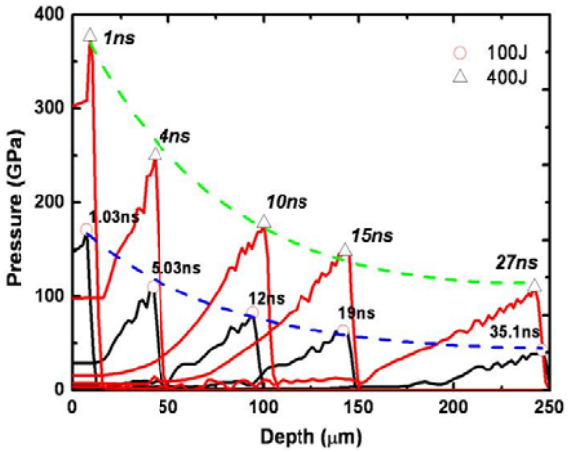

Figure 8:Shock wave propagated in Vanadium (250μm) (by HYADES): ○ and △ show shock wave with 100J and 400J initial energy propagation, respectively.

The dislocation behavior in MD does not give the same trend as in laser-shock experiments on nanocrystalline Ni [22, 23], where the grain sizes were between 30-50 nm. The samples in the experiments were prepared by electro-deposition at the Lawrence Livermore National Laboratory and were subjected to pressures between 20 and 70 GPa via laser. The microhardness of the samples after shock-compression was measured, and a 5-30 % increase after shock was observed, clearly indicating dislocation storage. Figure 7 (a) shows a cross-section of a sample with microhardness measurements taken at five positions beneath the cratered surface. Figure 7 (b) shows the increase in hardness

beneath the cratered surface (a maximum at position 3 occurs where laser intensity (i.e. deformation is greatest). In congruence with the hardness data, TEM examination revealed heavy dislocation activity ($\rho \sim 10^{16}$ m^2) due to laser shock and that full dislocations were the main carriers of plasticity. Interestingly, deformation twins were not observed in any of the samples, even at pressures up to 70 GPa.

4. FRAGMENTATION

Fragmentation was studied in monocrystalline and polycrystalline vanadium by means of laser compression followed by tension produced by reflection at the back surface. The experiments were carried out at the Janus Laser facility, at LLNL. The initial laser intensity was varied from 160 to 440 J. Figure 8 shows the predictions of pressure as the wave travels into the targets for laser intensities of 100 and 400 J. The significant decay of the wave is seen. The wave amplitudes after traveling 250 um into the target are only 1/3 of the initial values. Glass shields were placed at a specific distance behind the V targets were used to collect and analyze the ejected fragments in order to evaluate and quantify the extent of damage. The effects of target thickness, laser energy, and pulse duration were studied. Calculations show melting at a pressure threshold of ~150 GPa, which corresponds to a laser energy level of ~ 200 J. The recovered specimens and fragments show evidence of melting at the higher energy levels, consistent with the analytical predictions. Spallingin the monocrystalline V occurred with the formation of cleavage cracks oriented along {100}. Two perpendicular orientations are shown in Fig. 9a. The fracture in polycrystalline V occurred by a ductile tearing mechanism that favored grain boundaries, Fig. 9b. Experimentally obtained fragment sizes were compared with predictions from the Grady-Kipp model [26-28]. The spall strength of vanadium under laser loading conditions is calculated from the spall thickness.The theoretical prediction of fragment size, S, when solid spall is dominated by the flow stress, is given by the Grady-Kipp (G-K) theory for ductile materials. This theory is based on energetic considerations where the kinetic energy of an expanding body,*T*, and the elastic energy, *U*, are equated to a ductile fracture energy, $W=Y\varepsilon_c$:

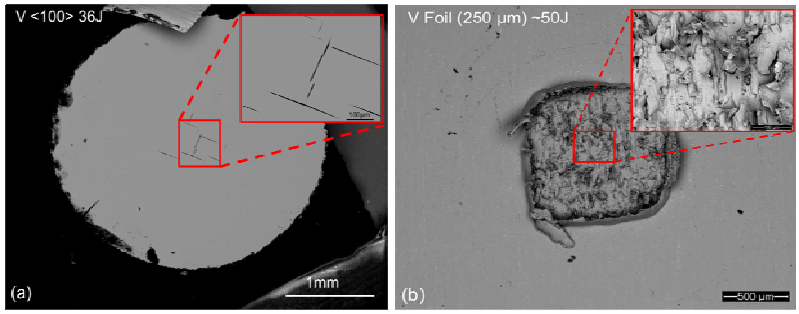

Figure 9: Spalling observation in V (vanadium) by SEM: (a) single crystal with <100> direction perpendicular to the surface; (b) polycrystal showing detailed microstructure in which grain-boundary separation is seen.(laser energy 50 J)

$$T + U \geq W \qquad (3)$$

This leads to: $$S = \left(\frac{6Y\varepsilon_c}{\rho \dot{\varepsilon}^2} \right)^{1/2} \qquad (4)$$

where Y is the dynamic yield stress, ρ is density, ε_c is the critical strain to failure, and $\dot{\varepsilon}$ is the imposed strain rate. The strain rate in the current experiments can be estimated from the expansion of the spalled region. The experimentally measured fragment sizes are shown in Figure 10 and compared with the Grady-Kipp predictions. The measured values are lower than the calculated ones but follow the same trend.

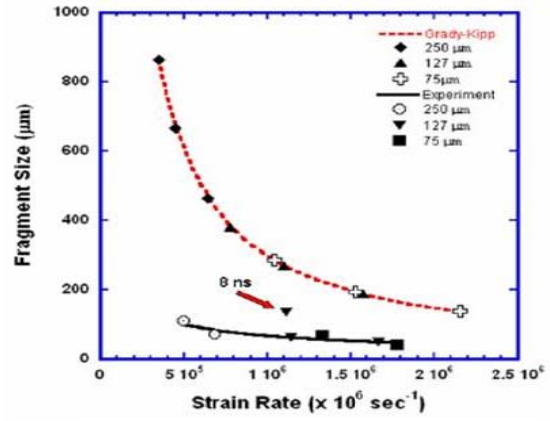

Figure 10: Fragment size vs. strain rate.

5. CONCLUSIONS

We have demonstrated that laser compression is a viable method to explore the dynamic response of metals to deformation and failure. The combined use of molecular dynamics and laser experiments can reveal new mechanisms and the limitations of old mechanisms. The homogeneous dislocation generation model [7] is confirmed by the molecular dynamics calculations, which also reveal that a large fraction of dislocations generated under compression are annihilated on release. In the compression of nanocrystalline Cu and Ni interganular shear is a prevalent deformation mode for grain sizes below 15 nm. Spalling experiments show that the presence of grain boundaries is important. Monocrystalline V has a higher spall strength than polycrystalline V. The Grady-Kipp [26-28] predictions of fragment sizes are compared with experimental values obtained in laser compression experiments. The fragment sizes experimentally obtained are smaller, by a factor of three, than the predictions from Grady-Kipp.

This research was funded by the UCOP under ILSA. We thank Dr. D. Correll for support and encouragement.

REFERENCES:

1. Smith C.S., Trans. AIME, Vol. 2 (1958), p. 212.
2. Weertman J., in Shock Waves and High-Strain-Rate Phenomena in Metals, eds. M.A. Meyers and L.E. Murr, Plenum, NY, (1981) p.469.
3. Weertman J., and FollansbeeP.S., Mech. Mater.,Vol. 2 (1983), p. 265.
4. Weertman J., Mech. Mater., Vol. 5 (1986), p. 13.
5. Johnson J.N., "Micromechanical Considerations in Shock Compression of Solids," in High-Pressure Shock Compression of Solids, eds., J. R. Asay and M. Shahinpoor, Springer-Verlag, NY, (1993) p. 249.
6. Johnson J.N., "Micromechanical Strength Effects in Shock Compression of Solid", in High-Pressure Science and Technology-1993, AIP, NY, (1994) p. 1145.
7. Meyers M.A.,Scripta Met., Vol. 12 (1978), p. 21.
8. Meyers M.A., in Strength of Metals and Alloys, eds., P. Haasen, et al., Pergamon, NY, 1979, p.547.
9. Zaretsky E., J. Appl. Phys., Vol. 78 (1995), p. 1.
10. Jarmakani H. N., McNaney J. M., Kad B., Orlikowski D., Nguyen J. H., and Meyers M. A., Mat. Sci.and Eng. A, Vol. 463 (2007),p. 249.
11. Jarmakani H. N., Bringa E. M., Earhart P., Remington B. A., Nhon V., And Meyers M. A., Acta Mat., Vol. 56 (2008), p. 5584.
12. Cao B., Bringa E. M., Meyers M. A., Met. Mat. Trans. A, Vol. 38 (2007), p. 2681.
13. Plimpton SJ. J Compute Phys,(1995); 117:1-19, http://lammps.sandia.gov.
14. Mishin Y., Farkas D., Mehl M. J., PapaconstantantopoulosD.A., Phys Rev B, Vol. 59 (1999), p. 3393.
15. Mishin Y., Mehl M.J., Papaconstantantopoulos D.A., Voter A.F. Phys. Rev. B, Vol. 63 (2001), p. 224106.
16. Daw M.S., Baskes M.I., Phys Rev Lett, Vol. 50 (1983), p. 1285.
17. Daw M.S., Baskes M.I., Phys Rev B, Vol. 29 (1984), p. 6443.
18. Kelchner C.L., Plimpton S., Hamilton J.C., Phys Rev B,Vol. 58 (1998), p. 11085.
19. Holian B.L., Lomdahl P.S., Science, Vol. 280 (1998), p.2085.
20. MurrL.E., in Shock Waves and High-Strain Rate Phenomena in metals, Plenum Press, New York, NY, (1981), pp. 607-73.
21. Chen M., Ma E., Hemker K.J., Sheng H., Wang Y., Cheng X., Science, Vol. 300 (2003), p. 1275.
22. Zhu Y.T., Liao X.Z., Srinivasan S.G., Zhao Y.G., Baskes M.I., Appl Phys Lett, Vol. 85 (2004), p. 5049.
23. Meyers M. A., Mishra A., Benson, D. J., Prog. Mat. Sci., Vol. 51 (2006), p. 427.
24. Wang Y.M., Bringa E.M., McNaney J.M., Victoria M., Caro A., Hodge A.M. Smith R., Torralva B., Remington B.A., Schuh C.A.,Jarmakani H., Meyers M.A., Appl Phys Lett, Vol. 88 (2006), p. 061917.
25. Wang Y.M., Bringa E.M., Victoria M., Caro A., McNaney J.M., Smith R., Remington B.A., J Phys IV France,Vol. 134 (2006), pp. 915-920.
26. Grady D.E., Kipp M.E., Int J Rock Mech Min Sci&Geomech, Vol. 17 (1979), p. 147.
27. Grady D.E., Kipp M.E., Int J Rock Mech Min Sci&Geomech, Vol. 16 (1979), p. 293.
28. Grady D.E., Kipp M.E., Mechs of Mats, Vol. 4 (1985), p. 311.

DYMAT 2009
Proceedings

BRUSSELS, BELGIUM, 7 – 11 SEPTEMBER 2009

EDP SCIENCES
17 avenue du Hoggar
PA de Courtabœuf, BP. 112
91944 Les Ulis Cedex A, France

Name of authors: **M. A. Meyers, H. Jarmakani, B. Y. Cao, C. T. Wei, B. Kad, B. A. Remington, E. M. Bringa, B. Maddox,D. Kalantar, D. Eder, A. Koniges**

Title of the communication: _____

_____

TRANSFER OF COPYRIGHT AGREEMENT

Must be filled in

Is hereby transferred to EDP Sciences (to the extent that it is transferable under applicable national laws), which will become effective when the article is accepted for publication.

Authors reserve the following rights:

1) All proprietary rights other than copyright, such as patent rights.
2) The right to grant or refuse permission to third parties to republish all or parts of the Paper or translations thereof. In the case where the entire Paper is republished, the third parties must also obtain EDP Sciences written permission.
3) The right to use all or part of this Paper in their future works.
4) In the case of a "work made for hire", the employer and the authors may make copies of this Paper for their own use, but not for resale.
5) An author may make his/her article published by EDP Sciences available on her/his personal site, her/his institution's web site and Open Archive Initiative sites, provided the source of the published article is cited and the ownership of the copyright clearly mentioned. These sites must be non for profit. Reprint and Postprint may be used (with the publisher's PDF). Authors are requested to create a link to the published article in the publisher internet service. The link must be accompanied by the following text "The original publication is available at www.edpsciences.org".

The author warrants that this contribution is original and he/she has full power to make this grant. To be signed by at least one of the authors (who agrees to inform the others, if any) or, in the case of a "work made for hire", by the employer.

Signature: Marc André Meyers

Print Name: Marc A. Meyers

Title (if not Author): Professor

Institute or Company: University of California, San Diego

Date: _____

An author who is a U.S. Government officer or employer and who prepared the submitted Paper as part of his or her official duties does not own any copyright in it. If at least one of the authors is not in this category, that author should sign above. If all the authors are in this category, check the box here and return this form unsigned.